Eur. Phys. J. C 18, 711–718 (2001)
Digital Object Identifier (DOI) 10.1007/s100520100572

**THE EUROPEAN PHYSICAL JOURNAL C**



# Anomalous $t$-dependence in diffractive electroproduction of $2S$ radially excited light vector mesons at HERA

J. Nemchik

Institute of Experimental Physics, Slovak Academy of Sciences, Watsonova 47, 04353 Košice, Slovakia

Received: 5 September 2000 / Revised version: 24 November 2000 /
Published online: 23 January 2001 – © Springer-Verlag 2001

**Abstract.** Within the color dipole gBFKL phenomenology of the diffraction slope we predict an anomalous $t$-dependence of the differential cross section $\mathrm{d}\sigma/\mathrm{d}t$ as a function of energy and $Q^2$ for the production of radially excited $V'(2S)$ light vector mesons. The pattern we found for the $t$-dependence for $\mathrm{d}\sigma/\mathrm{d}t$ is in contradiction with the well-known standard monotonical $t$-behavior for the $V(1S)$ vector mesons. The origin of this phenomenon lies in the interplay of the nodal structure of the $V'(2S)$ radial wave function and the energy and dipole size dependence of the color dipole cross section and the diffraction slope. We show how a different position of the node in the $V'(2S)$ wave function leads to a different pattern of anomalous $t$-behavior of $\mathrm{d}\sigma/\mathrm{d}t$ and discuss the possibility to determine this position from the low energy and HERA data.

## 1 Introduction

The diffractive photo- and electroproduction of ground state ($V(1S)$) and radially excited ($V'(2S)$) vector mesons,

$$\gamma^* p \to V(V')p \quad V = \rho, \Phi, \omega, J/\Psi, \Upsilon \cdots \\ (V' = \rho', \Phi', \omega', \Psi', \Upsilon' \cdots), \qquad (1)$$

at high c.m.s. energy $W = s^{1/2}$, intensively studied by the recent experiments at HERA, represents one of the main sources for the further development of pomeron physics. Pomeron exchange in the diffractive leptoproduction of vector mesons at high energies has been intensively studied [1–9] within the framework of perturbative QCD (pQCD).

The standard approach to pQCD is based on the BFKL equation [10–12], which represents the integral equation for the leading-log $s$ (LLs) evolution of the gluon distribution, formulated in the scaling approximation of the infinite gluon correlation radius $R_{\rm c} \to \infty$ (massless gluons) and of the fixed running coupling $\alpha_{\rm S} = \text{const}$. Later, however, a novel $s$-channel approach to the LLs BFKL equation (the running gBFKL approach) has been developed [13,14] in terms of the color dipole cross section $\sigma(\xi, r)$ (hereafter $r$ is the transverse size of the color dipole, $\xi = \log(W^2 + Q^2)/(m_V^2 + Q^2)$ is the rapidity variable) which consistently incorporates the asymptotic freedom (AF) (i.e. the running QCD coupling $\alpha_{\rm S}(r)$) and the finite propagation radius $R_{\rm c}$ of perturbative gluons. The freezing of $\alpha_{\rm S}(r)$, $\alpha_{\rm S}(r) \leq \alpha_{\rm S}^{\rm fr}$, and the gluon correlation radius $R_{\rm c}$ represent the nonperturbative parameters, which describe the transition from the soft (nonperturbative, infrared) to the hard (perturbative) region.

The details of the gBFKL phenomenology of diffractive electroproduction of light vector mesons are presented in [15]. The color dipole phenomenology of the diffraction slope for photo- and electroproduction of heavy vector mesons has been developed in [16]. The analysis of the diffractive production of light [6,15] and heavy [16] vector mesons at $t = 0$ within the gBFKL phenomenology shows that the $V(1S)$ vector meson production amplitude probes the color dipole cross section at the dipole size $r \sim r_S$ (*scanning phenomenon* [17,4–6]), where the scanning radius can be expressed through the scale parameter $A$:

$$r_{\rm S} \approx \frac{A}{\sqrt{m_V^2 + Q^2}}, \qquad (2)$$

where $Q^2$ is the photon virtuality, $m_V$ is the vector meson mass and $A \approx 6$. Consequently, changing $Q^2$ and the mass of the produced vector meson one can probe the dipole cross section $\sigma(\xi, r)$ and the dipole diffraction slope $B(\xi, r)$ and thus measure the effective intercept $\Delta_{\rm eff}(\xi, r) = \partial \log \sigma(\xi, r)/\partial\xi$ and the local Regge slope $\alpha'_{\rm eff}(\xi, r) = (1/2)\partial B(\xi, r)/\partial\xi$ in a very broad range of the dipole size $r$. This fact allows one to study the transition from large nonperturbative dipole size $r_{\rm S} \gg R_{\rm c}$ to the perturbative region of very short $r_{\rm S} \ll R_{\rm c}$.

The experimental investigation of the electroproduction of radially excited $V'(2S)$ vector mesons can provide additional information on the dipole cross section and the dipole diffraction slope.

The presence of the node in the $V'(2S)$ radial wave function leads to a strong cancellation of dipole size contributions to the production amplitude from the region above and below the node position $r_{\rm n}$ (the node effect [2,17,4, 18,15,16]). For this reason the amplitudes for the electroproduction of the $V(1S)$ and $V'(2S)$ vector mesons probe $\sigma(\xi,r)$ and $B(\xi,r)$ in a different way. The onset of a strong node effect has been demonstrated in [15], where the study of the electroproduction of $V'(2S)$ light vector mesons has shown a very spectacular pattern of anomalous $Q^2$ and energy dependence for the production cross section. For the electroproduction of $V'(2S)$ heavy vector mesons the node effect becomes much weaker but still leads to a slightly different $Q^2$- and energy dependence of the production cross section for $\Psi'$ versus $J/\Psi$ and to a nonmonotonical $Q^2$-dependence of the diffraction slope at small $Q^2 \lesssim 5\,{\rm GeV}^2$ for $\Psi'$ production [16]. Another manifestation of the node effect experimentally confirmed at HERA (and at fixed target experiments as well) in $J/\Psi$ and $\Psi'$ photoproduction is a strong suppression of the diffractive production of $V'(2S)$ versus $V(1S)$. The stronger the node effect, the smaller is the $V'(2S)/V(1S)$ ratio of the production cross sections. The node effect also leads to a counterintuitive inequality, $B(\gamma^*\to\Psi') \lesssim B(\gamma^*\to J/\Psi)$ [16], which can be tested at HERA. Therefore, it is very important to further explore the salient features of the node effect in conjunction with the emerging gBFKL phenomenology of the diffraction slope [19,20,16], especially in the production of $V'(2S)$ light vector mesons where the node effect is expected to be very strong. An anomalous energy and $Q^2$-dependence of the diffraction slope for the production of $V'(2S)$ light vector mesons has recently been studied in [21]. We found a correspondence between a specific nonmonotonic $Q^2$ and energy behavior of the diffraction slope and the position of the node in the $V'(2S)$ radial wave function. Moreover, we demonstrated that the above counterintuitive inequality found for the production of heavy vector mesons is not always valid for the production of light vector mesons.

In the present paper we concentrate on the model predictions for the differential cross sections ${\rm d}\sigma(\gamma^*\to V(1S))/{\rm d}t$ and ${\rm d}\sigma(\gamma^*\to V'(2S))/{\rm d}t$ at different energies and $Q^2$ and discuss for the first time how the explicit pattern of anomalous $t$ behavior of ${\rm d}\sigma(\gamma^*\to V'(2S))/{\rm d}t$ is connected with the position of the node in the radial wave function. We predict a strikingly different $t$-dependence of the differential cross section at different energies and $Q^2$ for the production of $V'(2S)$ versus $V(1S)$ vector mesons. The pattern we found for the anomalous $t$-behavior for ${\rm d}\sigma(\gamma^*\to V'(2S))/{\rm d}t$ can be tested at HERA.

This paper is organized as follows. In Sect. 2 we present a very short description of the color dipole phenomenology of diffractive photo- and electroproduction of vector mesons and the main results of the gBFKL phenomenology of the diffraction slope. In Sect. 3 we present the model predictions for the differential cross sections ${\rm d}\sigma(\gamma^*\to V(1S))/{\rm d}t$ and ${\rm d}\sigma(\gamma^*\to V'(2S))/{\rm d}t$ at different $Q^2$ and energies, and we discuss how the position of the node in the $V'(2S)$ radial wave function can be extracted from the data. The summary and conclusions are presented in Sect. 4.

## 2 Short review of the color dipole phenomenology for vector meson production and the diffraction slope

In the mixed $(\mathbf{r},z)$-representation the high energy meson is considered as a system of a color dipole described by the distribution of the transverse separation $\mathbf{r}$ of the quark and antiquark given by the $q\bar q$ wave function $\Psi(\mathbf{r},z)$, where $z$ is the fraction of the meson's light-cone momentum carried by a quark. The Fock state expansion for the relativistic meson starts with the $q\bar q$ state, and the higher Fock states $q\bar qg\cdots$ become very important at high energy. The interaction of the relativistic color dipole of the dipole size $\mathbf{r}$ with the target nucleon is quantified by the energy dependent color dipole cross section $\sigma(\xi,r)$ satisfying the gBFKL equation [13,14] for the energy evolution. This reflects the fact that in the leading-$\log 1/x$ approximation the effect of higher Fock states can be reabsorbed into the energy dependence of $\sigma(\xi,r)$. The dipole cross section is flavor independent and represents the universal function of $r$ which describes various diffractive processes in unified form. At high energy when the transverse separation $\mathbf{r}$ of the quark and antiquark is frozen during the interaction process, the scattering matrix describing the $q\bar q$–nucleon interaction becomes diagonal in the mixed $(\mathbf{r},z)$-representation ($z$ is known also as the Sudakov light-cone variable). This diagonalization property exists even when the dipole size $\mathbf{r}$ is large, i.e. beyond the perturbative region of short distances. The detailed discussion of the space-time pattern of diffractive electroproduction of vector mesons is presented in [16,15].

Following the advantage of the $(\mathbf{r},z)$-diagonalization of the $q\bar q$–$N$ scattering matrix, the imaginary part of the production amplitude for the real (virtual) photoproduction of vector mesons with momentum transfer $\mathbf{q}$ can be represented in the factorized form

$$\begin{aligned}{\rm Im}\mathcal{M}(\gamma^*\to V,\xi,Q^2,\mathbf{q}) &= \langle V|\sigma(\xi,r,z,\mathbf{q})|\gamma^*\rangle \\ &= \int\limits_0^1 {\rm d}z\int {\rm d}^2\mathbf{r}\sigma(\xi,r,z,\mathbf{q})\Psi_V^*(\mathbf{r},z)\Psi_{\gamma^*}(\mathbf{r},z) \quad (3)\end{aligned}$$

the normalization of which is ${\rm d}\sigma/{\rm d}t|_{t=0} = |\mathcal{M}|^2/16\pi$. In (3), $\Psi_{\gamma^*}(\mathbf{r},z)$ and $\Psi_V(\mathbf{r},z)$ represent the probability amplitudes to find a color dipole of size $r$ in the photon and quarkonium (vector meson), respectively. The color dipole distribution in (virtual) photons was derived in [22,13]. $\sigma(\xi,r,z,\mathbf{q})$ is the scattering matrix for the $q\bar q$–$N$ interaction and represents the above mentioned color dipole cross section for $\mathbf{q}=0$. The color dipole cross section $\sigma(\xi,r)$ depends only on the dipole size $r$. For small $\mathbf{q}$, as considered in this paper, one can safely neglect the $z$-dependence of $\sigma(\xi,r,z,\mathbf{q})$ for light and heavy vector meson production and set $z=1/2$. This follows partially from the analysis

within a double gluon exchange approximation [22] leading to a slow $z$-dependence of the dipole cross section.

The energy dependence of the dipole cross section is quantified in terms of the dimensionless rapidity $\xi = \log 1/x_{\rm eff}$; $x_{\rm eff}$ is the effective value of the Bjorken variable

$$x_{\rm eff} = \frac{Q^2 + m_V^2}{Q^2 + W^2} \approx \frac{m_V^2 + Q^2}{2\nu m_p}, \tag{4}$$

where $m_p$ and $m_V$ is the proton mass and mass of the vector meson, respectively. Hereafter, we will write the energy dependence of the dipole cross section in both variables, either in $\xi$ or in $x_{\rm eff}$ whatever seems convenient.

The production amplitudes for the transversely (T) and the longitudinally (L) polarized vector mesons with small momentum transfer $\mathbf{q}$ can be written in more explicit form [6,16]:

$$\begin{aligned}
&{\rm Im}\mathcal{M}_{\rm T}(x_{\rm eff}, Q^2, \mathbf{q}) \\
&= \frac{N_c C_V \sqrt{4\pi\alpha_{\rm em}}}{(2\pi)^2} \int {\rm d}^2\mathbf{r}\sigma(x_{\rm eff}, r, \mathbf{q}) \\
&\quad \times \int_0^1 \frac{{\rm d}z}{z(1-z)} \left\{ m_q^2 K_0(\varepsilon r)\phi(r,z) - [z^2 + (1-z)^2] \right. \\
&\quad \left. \times \varepsilon K_1(\varepsilon r)\partial_r\phi(r,z) \right\} \\
&= \frac{1}{(m_V^2 + Q^2)^2} \int \frac{{\rm d}r^2}{r^2} \frac{\sigma(x_{\rm eff}, r, \mathbf{q})}{r^2} W_{\rm T}(Q^2, r^2)
\end{aligned} \tag{5}$$

$$\begin{aligned}
&{\rm Im}\mathcal{M}_{\rm L}(x_{\rm eff}, Q^2, \mathbf{q}) \\
&= \frac{N_c C_V \sqrt{4\pi\alpha_{\rm em}}}{(2\pi)^2} \frac{2\sqrt{Q^2}}{m_V} \int {\rm d}^2\mathbf{r}\sigma(x_{\rm eff}, r, \mathbf{q}) \int_0^1 {\rm d}z \\
&\quad \times \left\{ [m_q^2 + z(1-z)m_V^2] K_0(\varepsilon r)\phi(r,z) - \partial_r^2\phi(r,z) \right\} \\
&= \frac{1}{(m_V^2 + Q^2)^2} \frac{2\sqrt{Q^2}}{m_V} \int \frac{{\rm d}r^2}{r^2} \frac{\sigma(x_{\rm eff}, r, \mathbf{q})}{r^2} W_{\rm L}(Q^2, r^2),
\end{aligned} \tag{6}$$

where

$$\varepsilon^2 = m_q^2 + z(1-z)Q^2; \tag{7}$$

$\alpha_{\rm em}$ is the fine structure constant, $N_c = 3$ is the number of colors, $C_V = 1/2^{1/2}$, $1/(3\sqrt{2})$, $1/3$, $2/3$, $1/3$ for $\rho^0$, $\omega^0$, $\phi^0$, $J/\Psi, \Upsilon$ production, respectively, and the $K_{0,1}(x)$ are the modified Bessel functions. The detailed discussion and parameterization of the light-cone radial wave function $\phi(r,z)$ of the $q\bar{q}$ Fock state of the vector meson is given in [15].

The terms $\propto \epsilon K_1(\epsilon r)\partial_r\phi(\mathbf{r},z)$ for (T) polarization and $\propto K_0(\epsilon r)\partial_r^2\Phi(\mathbf{r},z)$ for (L) polarization in the integrands of (5) and (6) represent the relativistic corrections; these become important at large $Q^2$ and for the production of light vector mesons. For the production of heavy quarkonia, the nonrelativistic approximation can be used with a rather high accuracy [2].

For small dipole size and $\mathbf{q} = 0$ in the leading-log $1/x$ approximation the dipole cross section can be related to the gluon structure function $G(x,q^2)$ of the target nucleon through

$$\sigma(x,r) = \frac{\pi^2}{3} r^2 \alpha_s(r) G(x,q^2), \tag{8}$$

where the gluon structure function enters at the factorization scale $q^2 \sim B/r^2$ [23] with the parameter $B \sim 10$ [24].

The weight functions $W_{\rm T}(Q^2,r^2)$ and $W_{\rm L}(Q^2,r^2)$ introduced in (5) and (6) have a smooth $Q^2$-behavior [6] and are very convenient for the analysis of the scanning phenomenon. They are sharply peaked at $r \approx A_{\rm T,L}/(Q^2 + m_V^2)^{1/2}$. At small $Q^2$ the values of the scale parameter $A_{\rm T,L}$ are close to $A \sim 6$, which follows from $r_{\rm S} = 3/\varepsilon$ with the nonrelativistic choice $z = 1/2$. In general, $A_{\rm T,L} \geq 6$ and increases slowly with $Q^2$ [6]. For the production of light vector mesons the relativistic corrections play an important role, especially at large $Q^2 \gg m_V^2$, and they lead to a $Q^2$-dependence of $A_{\rm L,T}$ coming from the large size asymmetric $q\bar{q}$-configurations $A_{\rm L}(\rho^0; Q^2 = 0) \approx 6.5$, $A_{\rm L}(\rho^0; Q^2 = 100\,{\rm GeV}^2) \approx 10$, $A_{\rm T}(\rho^0; Q^2 = 0) \approx 7$, $A_{\rm T}(\rho^0, Q^2 = 100\,{\rm GeV}^2) \approx 12$ [6]. Due to an extra factor $z(1-z)$ in the integrand of (6) in comparison with (5) the contribution from asymmetric $q\bar{q}$-configurations to the longitudinal meson production is considerably smaller.

The integrands in (5) and (6) contain the dipole cross section $\sigma(\xi, r, \mathbf{q})$. As was already mentioned, due to a very slow onset of the pure perturbative region (see (2)) one can easily anticipate a contribution to the production amplitude coming from the semiperturbative and nonperturbative $r \gtrsim R_{\rm c}$. Following the simplest assumption about the additive property of the perturbative and nonperturbative mechanism of interaction we can represent the contribution of the bare pomeron exchange to $\sigma(\xi, r, \mathbf{q})$ as a sum of the perturbative and nonperturbative components[1]:

$$\sigma(\xi, r, \mathbf{q}) = \sigma_{\rm pt}(\xi, r, \mathbf{q}) + \sigma_{\rm npt}(\xi, r, \mathbf{q}), \tag{9}$$

with the parameterization of both components at small $\mathbf{q}$

$$\begin{aligned}
&\sigma_{\rm pt,npt}(\xi, r, \mathbf{q}) = \\
&\sigma_{\rm pt,npt}(\xi, r, \mathbf{q} = 0) \exp\left( -\frac{1}{2} B_{\rm pt,npt}(\xi, r)\mathbf{q}^2 \right).
\end{aligned} \tag{10}$$

Here $\sigma_{\rm pt,npt}(\xi, r, \mathbf{q} = 0) = \sigma_{\rm pt,npt}(\xi, r)$ represent the contributions of the perturbative and nonperturbative mechanisms to the $q\bar{q}$–nucleon interaction cross section, respectively; $B_{\rm pt}(\xi, r)$ and $B_{\rm npt}(\xi, r)$ are the corresponding dipole diffraction slopes.

The small real part of the production amplitudes can be taken in the form [25]

$${\rm Re}\mathcal{M}(\xi, r) = \frac{\pi}{2} \frac{\partial}{\partial\xi} {\rm Im}\mathcal{M}(\xi, r), \tag{11}$$

and can easily be included in the production amplitudes (5) and (6) using the substitution

$$\begin{aligned}
\sigma(x_{\rm eff}, r, \mathbf{q}) &\to \left( 1 - {\rm i}\frac{\pi}{2} \frac{\partial}{\partial \log x_{\rm eff}} \right) \sigma(x_{\rm eff}, r) \\
&= [1 - {\rm i}\alpha_V(x_{\rm eff}, r)]\sigma(x_{\rm eff}, r, \mathbf{q}).
\end{aligned} \tag{12}$$

[1] The additive property of such a decomposition of the dipole cross section has been already discussed in [15,16]

The formalism for the calculation of $\sigma_{\rm pt}(\xi,r)$ in the leading-log $s$ approximation was developed in [22,13,14]. The contribution $\sigma_{\rm npt}(\xi,r)$ to the dipole cross section was used in [26,6,15,16], where we assumed that this soft nonperturbative component of the pomeron is a simple Regge pole with intercept $\Delta_{\rm npt}=0$. The particular form together with the assumption of the energy independent $\sigma_{\rm npt}(\xi=\xi_0,r)=\sigma_{\rm npt}(r)$ ($\xi_0$ corresponds to the boundary condition for the gBFKL evolution: $\xi_0=\log(1/x_0)$, $x_0=0.03$) allows one to successfully describe the proton structure function at very small $Q^2$ [26], the real photoabsorption [6] and the diffractive real and virtual photoproduction of light [15] and heavy [16] vector mesons. A larger contribution of the nonperturbative pomeron exchange to $\sigma_{\rm tot}(\gamma p)$ versus $\sigma_{\rm tot}(\gamma^* p)$ can, for example, explain the much slower rise with energy of the real photoabsorption cross section $\sigma_{\rm tot}(\gamma p)$ in comparison with $F_2(x,Q^2)\propto\sigma_{\rm tot}(\gamma^* p)$ observed at HERA [27,28]. Besides, the reasonable form of $\sigma_{\rm npt}(r)$ was confirmed in the process of the first determination of the dipole cross section from the data on vector meson electroproduction [29]. The energy and dipole size dependence of the extracted $\sigma(\xi,r)$ is in a good agreement with the dipole cross section obtained from the gBFKL dynamics [6,26]. The nonperturbative component of the pomeron exchange plays a dominant role at low NMC energies in the production of the light vector mesons, where the scanning radius $r_{\rm S}$, see (2), is large. However, the perturbative component of the pomeron becomes more important with the rise of energy also in the nonperturbative region of the dipole size.

If one starts with the familiar impact-parameter representation for the amplitude of elastic scattering of the color dipole,

$$\mathrm{Im}\mathcal{M}(\xi,r,\mathbf{q})=2\int \mathrm{d}^2\mathbf{b}\,\exp(-\mathrm{i}\mathbf{q}\mathbf{b})\Gamma(\xi,\mathbf{r},\mathbf{b}),\qquad(13)$$

then the diffraction slope $B=-2\mathrm{d}\log\mathrm{Im}\mathcal{M}/\mathrm{d}q^2|_{q=0}$ equals

$$B(\xi,r)=\frac{1}{2}\langle\mathbf{b}^2\rangle=\lambda(\xi,r)/\sigma(\xi,r),\qquad(14)$$

where

$$\lambda(\xi,r)=\int \mathrm{d}^2\mathbf{b}\mathbf{b}^2\Gamma(\xi,\mathbf{r},\mathbf{b}).\qquad(15)$$

The generalization of the color dipole factorization formula (3) to the diffraction slope of the reaction $\gamma^* p\to Vp$ reads

$$B(\gamma^*\to V,\xi,Q^2)\mathrm{Im}\mathcal{M}(\gamma^*\to V,\xi,Q^2,\mathbf{q}=0)$$
$$=\int\limits_0^1\mathrm{d}z\int\mathrm{d}^2\mathbf{r}\lambda(\xi,r)\Psi_V^*(r,z)\Psi_{\gamma^*}(r,z).\qquad(16)$$

The diffraction cone in the color dipole gBFKL approach for the production of vector mesons has been studied in detail in [16]. Here we only present the salient feature of the color diffraction slope emphasizing the presence of the geometrical contribution from the beam dipole, $r^2/8$, and the contribution from the target proton size, $R_N^2/3$:

$$B(\xi,r)=\frac{1}{8}r^2+\frac{1}{3}R_N^2+2\alpha'_{I\!P}(\xi-\xi_0)+\mathcal{O}(R_{\rm c}^2),\qquad(17)$$

where $R_N$ is the radius of the proton. For the electroproduction of light vector mesons the scanning radius is larger than the correlation one, $r\gtrsim R_{\rm c}$, even for $Q^2\lesssim 50\,\mathrm{GeV}^2$, and one recovers a sort of additive quark model, in which the uncorrelated gluonic clouds build up around the beam and target quarks and antiquarks and the term $2\alpha'_{I\!P}(\xi-\xi_0)$ describes the familiar Regge growth of the diffraction slope for the quark–quark scattering. The geometrical contribution to the diffraction slope from the target proton size $(1/3)R_N^2$ persists for all the dipole sizes $r\gtrsim R_{\rm c}$ and $r\lesssim R_{\rm c}$. The last term in (17) is also associated with the proton size and is negligibly small.

The soft pomeron and diffractive scattering of a large color dipole have also been studied in detail in [16]. Here we assume the conventional Regge rise of the diffraction slope for the soft pomeron [16]

$$B_{\rm npt}(\xi,r)=\Delta B_{\rm d}(r)+\Delta B_N+2\alpha'_{\rm npt}(\xi-\xi_0),\qquad(18)$$

where $\Delta B_{\rm d}(r)$ and $\Delta B_N$ stand for the contribution from the beam dipole and target nucleon size. As a guidance we take the experimental data on the pion–nucleon scattering [30], which suggest $\alpha'_{\rm npt}=0.15\,\mathrm{GeV}^{-2}$. In (18) the proton size contribution is

$$\Delta B_N=\frac{1}{3}R_N^2,\qquad(19)$$

and the beam dipole contribution has been proposed to have the form [16]

$$\Delta B_{\rm d}(r)=\frac{r^2}{8}\,\frac{r^2+aR_N^2}{3r^2+aR_N^2},\qquad(20)$$

where $a$ is a phenomenological parameter, $a\sim 1$. We take $\Delta B_N=4.8\,\mathrm{GeV}^{-2}$. Then the pion–nucleon diffraction slope is reproduced with a reasonable value of the parameter $a$ in (20): $a=0.9$ for $\alpha'_{\rm npt}=0.15\,\mathrm{GeV}^{-2}$.

Following the simple geometrical properties of the gBFKL diffraction slope $B(\xi,r)$ (see (17) and [19]) one can express its energy dependence through the energy dependent effective Regge slope $\alpha'_{\rm eff}(\xi,r)$

$$B_{\rm pt}(\xi,r)\approx\frac{1}{3}\langle R_N^2\rangle+\frac{1}{8}r^2+2\alpha'_{\rm eff}(\xi,r)(\xi-\xi_0).\qquad(21)$$

The effective Regge slope $\alpha'_{\rm eff}(\xi,r)$ varies with energy differently at different dipole sizes [19]. At fixed scanning radius and/or $Q^2+m_V^2$, it decreases with energy. At fixed rapidity $\xi$ and/or $x_{\rm eff}$, see (4), $\alpha'_{\rm eff}(\xi,r)$ rises with $r\lesssim 1.5\,\mathrm{fm}$. At fixed energy it is a flat function of the scanning radius. At asymptotically large $\xi$ ($W$), $\alpha'_{\rm eff}(\xi,r)\to\alpha'_{I\!P}=0.072\,\mathrm{GeV}^{-2}$. At lower and HERA energies the subasymptotic $\alpha'_{\rm eff}(\xi,r)\sim(0.15\text{–}0.20)\,\mathrm{GeV}^{-2}$ and is very close to $\alpha'_{\rm soft}$ known from the Regge phenomenology of soft scattering. This means that the gBKFL dynamics predicts

a substantial rise with the energy and dipole size of the diffraction slope $B(\xi,r)$ in accordance with the energy and dipole size dependence of the effective Regge slope $\alpha'_{\rm eff}(\xi,r)$ and due to the presence of the geometrical components $\propto r^2$ in (17) and $\Delta B_{\rm d}(r) \propto r^{1.7}$ in (18) (see also (20))[2]. The overall dipole diffraction slope contains contributions from both $B_{\rm npt}(\xi,r)$ and $B_{\rm pt}(\xi,r)$ and the corresponding geometrical component has $r^\alpha$-behavior with $1.7 < \alpha \lesssim 2.0$. Therefore, for discussions on the qualitative level in the subsequent section we assume (with a quite reasonable accuracy) an approximate $r^2$-dependence of the geometrical component contribution to the dipole diffraction slope.

Using the expressions (5) and (6) for the (T) and (L) production amplitudes in conjunction with (9), (10), (18) and (21) we can calculate the differential cross section of the vector meson electroproduction as a function of $t$.

## 3 Anomalous $t$-dependence of the differential cross section for the production of $V'(2S)$ vector mesons

The most important feature for $V'(2S)$ vector meson production is the node effect – the $Q^2$- and energy dependent cancellations from the soft (large size) and hard (small size) contributions (i.e. from the region above and below the node position, $r_{\rm n}$) to the $V'(2S)$ production amplitude. The strong $Q^2$-dependence of these cancellations comes from the scanning phenomenon (2) when the scanning radius $r_{\rm S}$ for some value of $Q^2$ is close to $r_{\rm n} \sim R_V$ ($R_V$ is the vector meson radius). The energy dependence of the node effect is due to a different energy dependence of the dipole cross section at small ($r < R_V$) and large ($r > R_V$) dipole sizes. We would like to emphasize from the very beginning that in the region of energy and $Q^2$ where the exact node effect is encountered the predictive power becomes weak and the predictions are strongly model dependent. The model predictions for $V'(2S)$ vector mesons presented in this section serve mostly as an illustration of a possible anomalous $Q^2$ and energy dependence[3].

There are several reasons to expect that for the production of $V'(2S)$ light vector mesons the node effect depends on the polarization of the virtual photon and of the produced vector meson [15]. First, the wave functions of (T) and (L) polarized (virtual) photons are different. Second, different regions of $z$ contribute to $\mathcal{M}_{\rm T}$ and $\mathcal{M}_{\rm L}$. Third, different scanning radii for the production of (T) and (L) polarized vector mesons and the different energy dependence of $\sigma(\xi,r)$ at these scanning radii lead to a different $Q^2$ and energy dependence of the node effect in the production of (T) and (L) polarized $V'(2S)$ vector mesons. Not so for the nonrelativistic limit of heavy quarkonia, where the node effect is very weak and is approximately polarization independent. There is only a weak polarization dependence of the node effect for $\Psi'$ production [16]. For $\Upsilon'$ production the node effect is negligibly small and is almost polarization independent.

There are two possible scenarios for the node effect which can occur in the $V'(2S)$ production amplitude: the undercompensation and the overcompensation scenario [18].

In the undercompensation scenario, the $V'(2S)$ production amplitude $\langle V'(2S)|\sigma(\xi,r)|\gamma^*\rangle$ is dominated by the positive contribution coming from small dipole sizes, $r \lesssim r_{\rm n}$, and the $V(1S)$ and $V'(2S)$ photoproduction amplitudes have the same sign. This scenario corresponds namely to the production of $V'(2S)$ heavy vector mesons $\Psi'(2S)$ and $\Upsilon'(2S)$. In the overcompensation scenario, the $V'(2S)$ production amplitude is dominated by the negative contribution coming from large dipole sizes, $r \gtrsim r_{\rm n}$, and the $V(1S)$ and $V'(2S)$ photoproduction amplitudes have opposite sign[4].

The anomalous properties of the diffraction slope were recently studied in [21] and come from the expression (16), which can be rewritten as the ratio of two matrix elements:

$$B(\gamma^* \to V(V'),\xi,Q^2) = \frac{\int\limits_0^1 {\rm d}z \int {\rm d}^2\mathbf{r}\Psi^*_{V(V')}(r,z)\sigma(\xi,r)B(\xi,r)\Psi_{\gamma^*}(r,z)}{\int\limits_0^1 {\rm d}z \int {\rm d}^2\mathbf{r}\Psi^*_{V(V')}(r,z)\sigma(\xi,r)\Psi_{\gamma^*}(r,z)}. \quad (22)$$

The production amplitude in the denominator of (22) is dominated by the contribution from the dipole size corresponding to the scanning radius $r_{\rm S}$ (2). However, due to the approximately $\propto r^2$ behavior of the dipole diffraction slope (see the discussion in Sect. 2), the integrand of the matrix element in the numerator of (22), is peaked by $r = r_B \sim 5/3 r_{\rm S} > r_{\rm S}$.

Let us discuss now the possible peculiarities in the $t$-dependence of the differential cross section ${\rm d}\sigma/{\rm d}t$ for the $V'(2S)$ production. Because of an approximate $\propto r^2$ behavior of the geometrical contribution to the diffraction slope, the large size negative contribution to the production amplitude from the region above the node position corresponds to a larger value of the diffraction slope than the small size contribution from the region below the node position. This means that the negative contribution to the $V'(2S)$ production amplitude has a steeper $t$-dependence than the positive contribution. This can be understood in a somewhat demonstrative form when the $t$-dependent production amplitude reads

[2] The dipole size behavior of $\Delta B_{\rm d}(r)$ (20) representing the geometrical contribution to the dipole diffraction slope $B_{\rm npt}(\xi,r)$ (18) for diffractive scattering of a large color dipole has the standard $r^2$-dependence at small, $r^2 \ll aR_N^2$, and large, $r^2 \gg aR_N^2$, values of the dipole size, respectively. In the intermediate region, $r^2 \sim aR_N^2$, which corresponds to the production of $V(1S)$ and $V'(2S)$ light vector mesons, the dipole size dependence of $\Delta B_{\rm d}(r)$ can be parameterized by the power function $r^\alpha$ with $\alpha \sim 1.7$

[3] Manifestations of the node effect in electroproduction on nuclei were discussed in [18,31]

[4] A discussion of the experimental determination of the relative sign of the $V'(2S)$ and $V(1S)$ production amplitudes using the so-called Söding–Pumplin effect [32,33] is presented in [15]

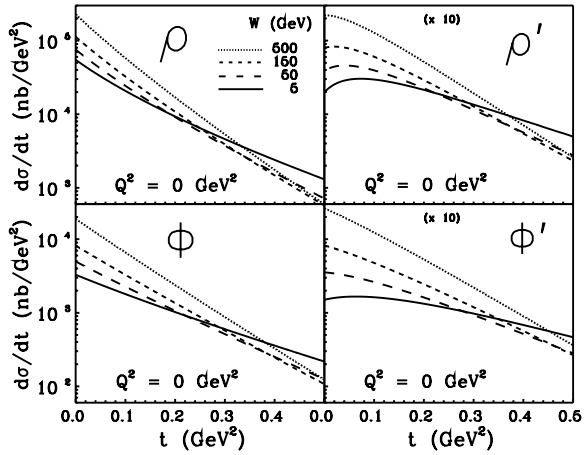


**Fig. 1.** The color dipole model predictions for the differential cross sections $\mathrm{d}\sigma(\gamma^* \to V(V'))/\mathrm{d}t$ for the real photoproduction ($Q^2 = 0$) of $\rho^0, \rho'(2S), \phi^0$ and $\phi'(2S)$ at different values of the c.m.s. energy $W$

$$\mathcal{M}(t) = \alpha \exp\left(-\frac{1}{2}B_1 t\right) - \beta \exp\left(-\frac{1}{2}B_2 t\right), \qquad (23)$$

where $\alpha$ and $\beta$ represent the contributions to the matrix element from the region below and above the node position with the corresponding effective diffraction slopes $B_1$ and $B_2$, respectively ($B_1 < B_2$). Consequently, the inequality $\alpha > \beta$ corresponds to the undercompensation whereas $\alpha < \beta$ is associated with the overcompensation regime. The destructive interference of these two contributions results in a decrease of the effective diffraction slope for the $V'(2S)$ meson production towards small $t$, contrary to the familiar increase for the $V(1S)$ meson production. Such a situation is shown in Fig. 1, where we present the model predictions for the differential cross section $\mathrm{d}\sigma(\gamma^* \to V(V'))/\mathrm{d}t$ for the production of the $V(1S)$ and $V'(2S)$ mesons at different c.m.s. energies $W$ and at $Q^2 = 0$. The real photoproduction measures the purely transverse cross section. Using the vector meson wave functions from [15] the forward production amplitude (3) is in the undercompensation regime (positive value). However, the matrix element in the numerator of (22) is safely in the overcompensation regime (negative value) (at $W \lesssim 150\,\mathrm{GeV}$ for $\rho'(2S)$ production and at $W \lesssim 30\,\mathrm{GeV}$ for $\phi'(2S)$ production) because of $r_B > r_S$. As the result, we predict the negative value diffraction slope at $t = 0$ and $Q^2 = 0$. At $t > 0$ the node effect becomes weaker. The higher $t$, the weaker is the node effect as a consequence of the destructive interference discussed above. Consequently, the differential cross section first rises with $t$, and flattens off at $t \in (0.0\text{–}0.2)\,\mathrm{GeV}^2$, having a broad maximum. At large $t$, the node effect is weak and $\mathrm{d}\sigma(\gamma^* \to V'(2S))/\mathrm{d}t$ decreases with $t$ monotonically as for $V(1S)$ production. The position of the maximum can be roughly evaluated from (23) and reads

$$t_{\max} \sim \frac{1}{B-A} \log\left[\frac{\beta^2}{\alpha^2}\frac{B^2}{A^2}\right], \qquad (24)$$

with the supplementary condition

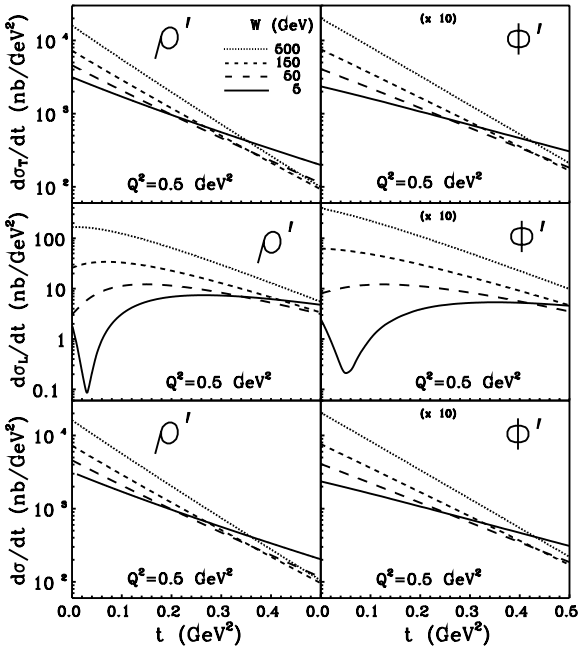


**Fig. 2.** The color dipole model predictions for the differential cross sections $\mathrm{d}\sigma_{\mathrm{L,T}}(\gamma^* \to V'(2S))/\mathrm{d}t$ for transversely (T) (top boxes) and longitudinally (L) (middle boxes) polarized radially excited $\rho'(2S)$, $\phi'(2S)$ and for the polarization-unseparated $\mathrm{d}\sigma(\gamma^* \to V')/\mathrm{d}t = \mathrm{d}\sigma_{\mathrm{T}}(\gamma^* \to V'(2S))/\mathrm{d}t + \epsilon \mathrm{d}\sigma_{\mathrm{L}}(\gamma^* \to V'(2S))/\mathrm{d}t$ for $\epsilon = 1$ (bottom boxes) at $Q^2 = 0.5\,\mathrm{GeV}^2$ and different values of the c.m.s. energy $W$

$$\frac{\beta}{\alpha} > \frac{A}{B}, \qquad (25)$$

where $A = 2B_1$ and $B = 2B_2$, $A < B$. If the condition (25) is not fulfilled, $\mathrm{d}\sigma(\gamma^* \to V'(2S))/\mathrm{d}t$ has no maximum and exhibits a standard monotonical $t$-behavior as for the production of $V(1S)$ mesons.

The predicted nonmonotonic $t$-behavior of the differential cross section for $\rho'(2S)$ and $\phi'(2S)$ production in the photoproduction limit is strikingly different, especially at smaller energies, from the familiar decrease with $t$ of $\mathrm{d}\sigma(\gamma \to \rho^0(1S))/\mathrm{d}t$ and $\mathrm{d}\sigma(\gamma \to \phi^0(1S))/\mathrm{d}t$ (see Fig. 1). Here we cannot insist on the precise form of the $t$-dependence of the differential cross sections; the main emphasis is on the likely pattern of the $t$-dependence coming from the node effect.

At larger energies, $W \gtrsim 150\,\mathrm{GeV}$ for the $\rho'(2S)$ photoproduction and $W \gtrsim 30\,\mathrm{GeV}$ for $\phi'(2S)$ photoproduction, the node effect becomes weaker and we predict the positive value diffraction slope at $t = 0$ because both the matrix elements in (22) are positive valued. For this reason, the nonmonotonic $t$-dependence of the differential cross section is exchanged for the monotonic one, but still the effective diffraction slope decreases slightly towards small $t$ (see Fig. 1).

Because of a possible overcompensation scenario for $\rho'_{\mathrm{L}}(2S)$ and $\phi'_{\mathrm{L}}(2S)$ mesons in the forward direction ($t = 0$) and at small $Q^2$ (see [15]), we present in Fig. 2 the model predictions for $\mathrm{d}\sigma(\gamma^* \to V'(2S))/\mathrm{d}t$ at different energies $W$ and at fixed $Q^2 = 0.5\,\mathrm{GeV}^2$ for the produc-

tion of (T), (L) polarized and polarization-unseparated $\rho'(2S)$ and $\phi'(2S)$ mesons. As was mentioned above, at $Q^2 = 0.5\,\mathrm{GeV}^2$, the node effect becomes weaker, the amplitudes for both $\rho'_{\mathrm{T}}(2S)$ and $\phi'_{\mathrm{T}}(2S)$ production at $t = 0$ are in the undercompensation regime and the corresponding slope parameters $B(\rho'_{\mathrm{T}}(2S))$ and $B(\phi'_{\mathrm{T}}(2S))$ have a positive value. For this reason, we predict the familiar $t$-dependence of $\mathrm{d}\sigma(\gamma^* \to V'_{\mathrm{T}}(2S))/\mathrm{d}t$ (see bottom boxes in Fig. 2). The above mentioned maximum of $\mathrm{d}\sigma/\mathrm{d}t$ is absent because of a weaker node effect and consequently the condition (25) is not fulfilled.

However, at $Q^2 \lesssim 0.5\,\mathrm{GeV}^2$, the production amplitude for $\rho'_{\mathrm{L}}(2S)$ and $\phi'_{\mathrm{L}}(2S)$ in the forward direction (and the matrix element $\langle V'_{\mathrm{L}}(2S)|\sigma(\xi,r)B(\xi,r)|\gamma^*\rangle$ as well) is still in the overcompensation regime and the corresponding diffraction slope $B(V'_{\mathrm{L}}(2S))$ has a positive value at small energies, $W \lesssim 20\,\mathrm{GeV}$. This results in the very spectacular pattern of anomalous $t$-dependence for $\mathrm{d}\sigma(\gamma^* \to V'_{\mathrm{L}}(2S))/\mathrm{d}t$ shown in Fig. 2 (middle boxes). With rising $t$ due to the above described destructive interference of two contributions to the production amplitude with different $t$-dependences (see (23)), one encounters the exact node effect at some $t \sim t_{\min}$. Consequently, the differential cross section first falls rapidly with $t$, having a minimum at $t \sim t_{\min}$. At still larger $t$, when the overcompensation scenario of the $t$-dependent production amplitude is changed for the undercompensation one and the slope parameter becomes negatively valued, $\mathrm{d}\sigma(\gamma^* \to V'_{\mathrm{L}}(2S))/\mathrm{d}t$ rises with $t$ and the further pattern of the $t$-behavior is analogous to that for $V'_{\mathrm{T}}(2S)$ production (see Fig. 1).

The position of the minimum in the differential cross section is model dependent and can be roughly estimated from (23):

$$t_{\min} \sim \frac{1}{B-A}\log\left[\frac{\beta^2}{\alpha^2}\right]. \tag{26}$$

The gBFKL model predictions give $t_{\min} \sim 0.03\,\mathrm{GeV}^2$ for $\rho'_{\mathrm{L}}(2S)$ production and $t_{\min} \sim 0.05\,\mathrm{GeV}^2$ for $\phi'_{\mathrm{L}}(2S)$ production at $Q^2 = 0.5\,\mathrm{GeV}^2$ and at $W = 5\,\mathrm{GeV}$. However, we cannot exclude the possibility that this minimum will be placed at other values of $t$. At $Q^2 < 0.5\,\mathrm{GeV}^2$, $t_{\min}$ reaches larger values of $t$. At higher energy, the position of $t_{\min}$ is shifted to a smaller value of $t$ unless the exact node effect is reached at $t = 0$. At still larger energy, when the $V'_{\mathrm{L}}(2S)$ production amplitude is in the undercompensation regime, this minimum disappears and we predict the pattern of $t$-behavior for $\mathrm{d}\sigma(\gamma^* \to V'_{\mathrm{L}}(2S))/\mathrm{d}t$ analogous to that for $\mathrm{d}\sigma(\gamma \to V'_{\mathrm{T}}(2S))/\mathrm{d}t$ in the photoproduction limit described in Fig. 1. These predicted anomalies can be tested at HERA measuring the diffractive electroproduction of $V'(2S)$ light vector mesons in the separate (T) and (L) polarizations.

## 4 Conclusions

We study the diffractive photo- and electroproduction of the ground state $V(1S)$ and radially excited $V'(2S)$ vector mesons within the color dipole gBFKL dynamics with the main emphasis on the differential cross section $\mathrm{d}\sigma/\mathrm{d}t$. There are two main consequences of vector meson production coming from the gBFKL dynamics.

First, the energy dependence of the $V(1S)$ vector meson production is controlled by the energy dependence of the dipole cross section which is steeper for smaller dipole sizes. The energy dependence of the diffraction slope for $V(1S)$ production is given by the effective Regge slope with a small variation with energy.

Second, the $Q^2$-dependence of the $V(1S)$ vector meson production is controlled by the shrinkage of the transverse size of the virtual photon and the small dipole size dependence of the color dipole cross section. The $Q^2$-behavior of the diffraction slope is given by the geometrical contribution with an approximate $\sim r^2$ behavior coming from the color dipole gBFKL phenomenology of the slope parameter.

As a consequence of the node in the $V'(2S)$ radial wave function, we predict a strikingly different $t$-dependence of the differential cross section for the production of $V'(2S)$ versus $V(1S)$ vector mesons. The origin of this is in the destructive interference of the large distance negative contribution to the production amplitude from the region above the node position with a steeper $t$-dependence and the small distance positive contribution to the production amplitude from the region below the node position with a weaker $t$-dependence. As a result, we predict at $Q^2 = 0$ a nonmonotonic $t$-dependence of $\mathrm{d}\sigma(\gamma \to V'_{\mathrm{T}}(2S))/\mathrm{d}t$ and a decreasing diffraction slope for $V'_{\mathrm{T}}(2S)$ mesons towards small values of $t$ in contrast with the familiar increase for the $V(1S)$ mesons. The differential cross section $\mathrm{d}\sigma(\gamma \to V'_{\mathrm{T}}(2S))/\mathrm{d}t$ first rises with $t$, having a broad maximum at $t \sim t_{\max}$ as given by (24). The position of the maximum is model dependent and is shifted to smaller values of $t$ with rising energy and $Q^2$ due to a weaker node effect. At larger $t$ when the node effect is still weaker, $\mathrm{d}\sigma(\gamma \to V'_{\mathrm{T}}(2S))/\mathrm{d}t$ has the standard monotonic $t$-behavior as for the production of $V(1S)$ vector mesons. This pattern of the anomalous $t$-dependence of $\mathrm{d}\sigma(\gamma \to V'_{\mathrm{T}}(2S))/\mathrm{d}t$ corresponds to the undercompensation scenario for the production amplitude.

For the production of (L) polarized $V'_{\mathrm{L}}(2S)$ mesons, there is overcompensation at $t = 0$ leading to an exact cancellation of the positive contribution from large size dipoles and the negative contribution from small size dipoles to the production amplitude and to a minimum of the differential cross section at some value of $t \sim t_{\min}$. The position of $t_{\min}$ is given by (25), is energy dependent, and leads to a complicated pattern of anomalous $t$-dependence for $\mathrm{d}\sigma(\gamma^* \to V'_{\mathrm{L}}(2S))/\mathrm{d}t$ at fixed $Q^2$. Consequently, $\mathrm{d}\sigma(\gamma^* \to V'_{\mathrm{L}}(2S))/\mathrm{d}t$ first falls with $t$ having a minimum at $t \sim t_{\min}$ when the overcompensation scenario is changed for the undercompensation one. The following pattern of $t$-behavior is then analogous to $\mathrm{d}\sigma(\gamma \to V'_{\mathrm{T}}(2S))/\mathrm{d}t$ at $Q^2 = 0$. These anomalies are also energy and $Q^2$-dependent and can be tested at HERA.

The experimental investigation of the $t$-dependent differential cross section for real photoproduction ($Q^2 = 0$) of $V'(2S)$ vector mesons at fixed target and HERA exper-

iments offers an unique possibility to make a choice between the undercompensation and overcompensation scenarios. The presence of the minimum in $\mathrm{d}\sigma(\gamma \to V'(2S))/\mathrm{d}t$ for a broad energy range corresponds to the overcompensation scenario. Otherwise, the $V'(2S)$ production amplitude is in the undercompensation scenario.

The position of the node in the radial $V'(2S)$ wave function can be tested also by the vector meson data with the separate (L) and (T) polarizations at $Q^2 > 0$. The existence of a dip (minimum) (for a broad energy range) in the $t$-dependent differential cross section is connected again with the overcompensation scenario in the $V'(2S)$ production amplitude. The broad maximum and/or the standard monotonic $t$-behavior of $\mathrm{d}\sigma/\mathrm{d}t$ leads one to prefer the undercompensation scenario.

## References


1. A. Donnachie, P.V. Landshoff, Phys. Lett. B **185**, 403 (1987); J.R. Cuddell, Nucl. Phys. B **336**, 1 (1990)
2. B.Z. Kopeliovich, B.G. Zakharov, Phys. Rev. D **44**, 3466 (1991)
3. M.G. Ryskin, Z. Phys. C **57**, 89 (1993)
4. B.Z. Kopeliovich, J. Nemchik, N.N. Nikolaev, B.G. Zakharov, Phys. Lett. B **309**, 179 (1993)
5. B.Z. Kopeliovich, J. Nemchik, N.N. Nikolaev, B.G. Zakharov, Phys. Lett. B **324**, 469 (1994)
6. J. Nemchik, N.N. Nikolaev, B.G. Zakharov, Phys. Lett. B **341**, 228 (1994)
7. S.J. Brodsky et al., Phys. Rev. D **50**, 3134 (1994)
8. J.R. Forshaw, M.G. Ryskin, Z. Phys. C **68**, 137 (1995)
9. E. Gotsman, E.M. Levin, U. Maor, Nucl. Phys. B **464**, 251 (1996)
10. E.A. Kuraev, L.N. Lipatov, S.V. Fadin, Sov. Phys. JETP **44**, 443 (1976); **45**, 199 (1977)
11. Yu.Yu.Balitsky, L.N. Lipatov, Sov. J. Nucl. Phys. **28**, 822 (1978)
12. L.N. Lipatov, Sov. Phys. JETP **63**, 904 (1986); L.N. Lipatov, in: Perturbative Quantum Chromodynamics, edited by A.H. Mueller (World Scientific 1989)
13. N. Nikolaev, B.G. Zakharov, JETP **78**, 598 (1994); Z. Phys. C **64**, 631 (1994)
14. N.N. Nikolaev, B.G. Zakharov, V.R. Zoller, JETP Letters **59**, 6 (1994); JETP **78**, 866 (1994); Phys. Lett. B **328**, 486 (1994)
15. J. Nemchik, N.N. Nikolaev, E. Predazzi, B.G. Zakharov, Z. Phys C **75**, 71 (1997)
16. J. Nemchik, N.N. Nikolaev, E. Predazzi, B.G. Zakharov, V.R. Zoller, JETP **86**, 1054 (1998)
17. N.N. Nikolaev, Comments on Nucl. Part. Phys. **21**, 41 (1992)
18. J. Nemchik, N.N. Nikolaev, B.G. Zakharov, Phys. Lett. B **339**, 194 (1994)
19. N.N. Nikolaev, B.G. Zakharov, V.R. Zoller, Phys. Lett. B **366**, 337 (1996)
20. N.N. Nikolaev, B.G. Zakharov, V.R. Zoller, JETP Lett. **60**, 694 (1994)
21. J. Nemchik, The wave function of $2S$ radially excited vector mesons from data for diffraction slope, hep-ph 0003245, submitted to Phys. Rev. D
22. N.N. Nikolaev, B.G. Zakharov, Z. Phys. C **49**, 607 (1991); Z. Phys. C **53**, 331 (1992)
23. V. Barone, M. Genovese, N.N. Nikolaev, E. Predazzi, B.G. Zakharov, Z. Phys. C **58**, 541 (1993); Int. J. Mod. Phys. A **8**, 2779 (1993)
24. N.N. Nikolaev, B.G. Zakharov, Phys. Lett. B **332**, 184 (1994)
25. V.N. Gribov, A.A. Migdal, Sov. J. Nucl. Phys. **8**, 703 (1969)
26. N.N. Nikolaev, B.G. Zakharov, Phys. Lett. B **327**, 149 (1994)
27. H1 Collab., I. Abt et al., Nucl. Phys. B **407**, 515 (1993)
28. ZEUS Collab., M. Derrick et al., Phys. Lett. (1993)
29. J. Nemchik, N.N. Nikolaev, E. Predazzi, B.G. Zakharov, Phys. Lett. B **374**, 199 (1996)
30. A. Schiz et al., Phys. Rev. D **24**, 26 (1981); J.P. Burq et al., Phys. Lett. B **109**, 111 (1982)
31. O. Benhar, B.G. Zakharov, N.N. Nikolaev et al., Phys. Rev. Lett. **74**, 3565 (1995); O. Benhar, S. Fantoni, N.N. Nikolaev et al., Zh. Exp. Teor. Fiz. **111**, 769 (1997)
32. P. Söding, Phys. Lett. **19**, 702 (1966)
33. J. Pumplin, Phys. Rev. D **2**, 1859 (1970)